AIAA-2003-4010

Hydrodynamic Prediction of High Speed Microflows

Reni Raju and Subrata Roy
Computational Plasma Dynamics Laboratory
Kettering University
Flint, MI 48504

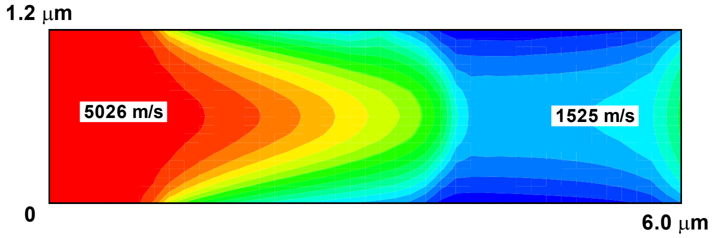

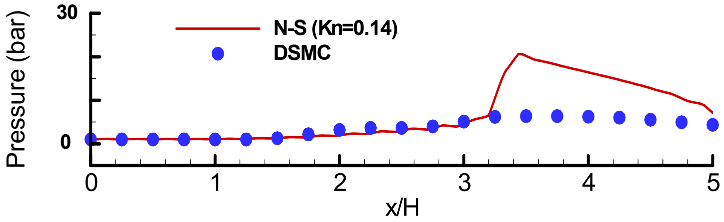

33rd AIAA Fluid Dynamics Conference & Exhibit

23 - 26 Jun 2003
Orlando, Florida

33rd AIAA FLUID DYNAMICS CONFERENCE AND EXHIBIT
23 - 26 Jun 2003
Orlando, Florida

Hydrodynamic Prediction of High Speed Microflows

Reni Raju[*] and **Subrata Roy**[†]
Computational Plasma Dynamics Laboratory
Department of Mechanical Engineering
Kettering University, Flint, Michigan 48504, USA

Characteristics of gas flow in the transition regime are presented for microchannels for both subsonic and supersonic flows. A low speed pressure driven flow and two high speed flow cases through microchannels have been documented using a hydrodynamic finite element formulation with first order slip/jump boundary conditions. The subsonic flow case uses a channel of aspect ratio 5639, while for the high speed flow the microchannel has an aspect ratio of 5. Presented subsonic flow results are benchmarked with experiment and reported numerical model. The solution profiles for supersonic micro flow cases are compared to the published DSMC results. Numerical solution of the hydrodynamic model documents excellent shock capturing capability.

NOMENCLATURE

C_p	Specific heat at constant pressure
γ	Specific heat ratio
λ	Mean free path of the fluid
k	Thermal conductivity
Kn	Knudsen Number
Ma_0	Reference Mach number
μ	Coefficient of viscosity
Pr	Prandtl number
P	Gas pressure
P_0	Reference pressure
ρ	Gas density
ρ_0	Reference density
R	Reduced gas constant
σ_v	Tangential-momentum-coefficient
σ_T	Thermal-momentum-coefficient
t	Time
T	Gas temperature
T_0	Reference temperature
T_w	Wall temperature
u	Gas velocity in x-direction
u_0	Reference velocity
v	Gas velocity in y-direction

INTRODUCTION

Past two decades have found a vast improvement in micromachining techniques that fostered rapid development in micro-electromechanical systems (MEMS) and nano-eletromechanical systems (NEMS). A wide variety of micro scale devices like sensors, actuators and valves have been developed for applications in biomedical, electronics, aerospace and automobile industry. A few of the MEMS devices have also been designed for fluid applications like micro-pumps, micro-valves, micro-turbines, microthrusters etc. This emerging trend has generated strong interest in understanding physical laws governing these systems. The transport phenomenon in microdevices is fundamentally different from that in macroscale devices due to the change in length scale. The mean free path of the gas at atmospheric conditions is of the order of $\sim 10^{-8}$ m. As the physical dimensions of a system become comparable to the mean free path, the gas flow becomes rarefied. For liquids however, the flow becomes granular and involve effects of surface forces[1], adsorption, wetting and electrokinetics[2].

---

[*] Graduate Student, Email: raju8515@kettering.edu, Student member, AIAA.

[†] Associate Professor, Email: sroy@kettering.edu, Associate Fellow, AIAA.

In general, numerical modeling of fluid flow is carried out using either the continuum or the molecular approach. The continuum approach is used widely for its efficiency and easy implementation. However, as the length scale of a physical system (Λ) approaches the mean free path (λ) of the fluid, the validity of the standard continuum approach with no-slip boundary conditions diminishes. The degree of rarefaction and the applicability of the continuum model is determined by the local value of a non-dimensional parameter, called Knudsen number and $\mathrm{Kn} = \lambda/\Lambda = 16\mu/5\rho\sqrt{2\pi RT}$ (based on the Chapman-Enskog result). As Kn → 0, the flow can be assumed sufficiently continuous while for Kn > 10 it becomes a free-molecule flow[3]. However, for 0.001 < Kn < 10 the flow is neither sufficiently continuum nor completely molecular. Thus, this regime can be further divided into two subcategories; slip-flow for 0.001 < Kn < 0.1 and transition for 0.1 < Kn < 10.

Several experiments have been carried out to study various aspects of fluid flow through microchannels. Pfahler *et al.*[4] and Harley *et al.*[5] have conducted experiments for low Reynolds number flows. Liu *et al.* [6], Pong *et al.* [7] and Shih *et al.*[8] have measured both pressure distribution and mass flow rate for different gas flows through surface and bulk micromachined microchannels. Arkilic *et al.*[9-10] have conducted similar experiments for microchannels of different dimensions. Most of these experiments are based on subsonic or pressure driven flows having low Reynolds number. However for some particular applications like in the aerospace industry high speed flows maybe encountered.

The reported numerical modeling of high speed flows in literature is generally simulated with direct simulation Monte Carlo[11] or Burnett equation models[12]. Supersonic flows having a range of Kn from 0.004 to 0.19 have been simulated using DSMC[13-15]. Similar results using the augmented Burnett equations have also been published[16]. The molecular approach using molecular dynamics and DSMC provides reasonably accurate solutions for micro flows but are restrictive due to high computation cost and the impractical CPU time requirement.[2,13,17] In addition obtaining realistic solutions for channels with higher aspect ratios becomes increasingly difficult[13,18].In general, to understand the system the primary aim in microscale simulation is to know the average quantities of the velocity and mass flux rather than molecular quantities. A more feasible approach is considering the bulk properties for the fluid flow while accommodating the different effects encountered in microfluidics like the wall-slip/jump, compressibility, rarefaction and thermal creep, thus yielding a closer approximation to the overall behavior of the flow in the domain at lower computational cost and reduced turnaround time.

It has been reported that the Navier-Stokes equations with first order velocity-slip[19] and temperature-jump[20] boundary conditions work well for the slip-flow regime (0.001< Kn < 0.1). Higher order boundary conditions[2] are suggested when the flow becomes transitional (0.1< Kn < 10). However first order equations can also reasonably predict solutions in both slip and transition regime.[21,22] A two-dimensional finite element based code is being developed at Computational Plasma Dynamics Laboratory (CPDL) for micro and nano[21] flow applications. As a preliminary case study we have investigated the fluid flow inside a microthruster[23] and a subsonic Poiseuille flow inside a microchannel for the slip-flow regime (outlet Kn = 0.0585) using first order boundary conditions.[21] The channel pressure distribution solution and predicted mass fluxes have been accurately validated with published experimental data[6] and numerical results.[24]

As a complement to our previous report[21], this paper aims to extend the applicability of the developed hydrodynamic model to both low and high speed slip and transitional flows. The subsonic flow involves flow through a microchannel with a high aspect ratio by Arkilic *et al*[9]. The Knudsen number at the outlet is 0.155 for this case. The two important aspects of high speed flows are the fluid flow and heat transfer characteristics. The results for heat transfer properties are presented separately. The high-speed fluid flow results are presented for the values of the Knudsen number ranging from 0.062-0.14 (slip-transitional). The solutions have been compared with reported DSMC results.[13,14]

MODEL

The first case is the subsonic pressure driven flow through a microchannel of aspect ratio **L/H** = 5639. The second case is a two-dimensional model which is an extension of the experimental study of pressure driven flows by Pong *et al.*[7] The geometric conditions[7] have been modified by Oh *et al.*[13] changing the aspect ratio from 2500 to 5, in order to obtain hypersonic flow conditions for working fluid helium. The channel geometry for Case 3 presented by Liou *et al.*[14] is similar to that of Case 2 but for the working fluid nitrogen. For these two high speed cases a free stream region ***B*** is specified near the inlet section of the microchannel as shown in Figure 1. The microchannel dimensions and flow parameters for all three cases are enlisted in the Table 1. The three-dimensional end effects have been neglected for this analysis.

	Case 1	***Case 2***	***Case 3***
Fluid	Helium	Helium	Nitrogen
L (*μm*)	7500.0	6.0	6.0
H (*μm*)	1.33	1.2	1.2
B (*μm*)	-	1.0	0.6
Kn	0.155	0.062	0.14
T_0 (*K*)	314	300	298
T_w (*K*)	314	323	298
Ma_0	-	4.15	5.0
P_{in}/P_{out}	1.34,1.68,2.02, 2.36, 2.701	-	-
P_0 (*Pa*)	1.01×10^5	1.01×10^5	1.01×10^5
R (*J/kg.K*)	2076.9	2076.9	296.8
C_p(*J/kg.K*)	5192.6	5192.6	1039.0
μ (*N-s/m*^{2})	2.06×10^{-5}	2.06×10^{-5}	1.85×10^{-5}
k (*W/k.m*)	0.152	0.152	0.0259
γ	1.667	1.667	1.40

Table 1: Model dimensions and flow conditions.

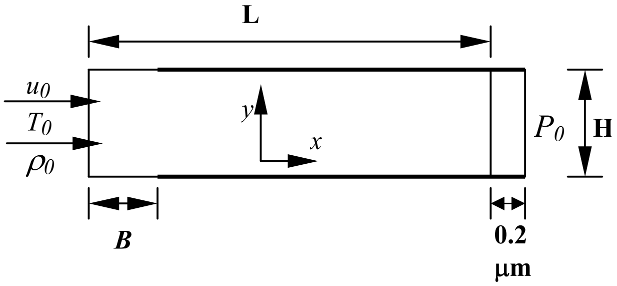

Figure 1: Schematic of microchannel geometry for high speed flow.[13]

GOVERNING EQUATIONS

The standard two-dimensional, time-dependent, compressible Navier-Stokes form with constant viscosity is used to analyze the gas flow through microchannels.

Conservation of Mass:

$$\frac{\partial \rho}{\partial t} + \frac{\partial \rho u}{\partial x} + \frac{\partial \rho v}{\partial y} = 0 \tag{1}$$

Conservation of x- momentum:

$$\frac{\partial \rho u}{\partial t} + u\frac{\partial \rho u}{\partial x} + v\frac{\partial \rho u}{\partial y} + \frac{\partial P}{\partial x} - \mu\left(\frac{\partial^2 u}{\partial x^2} + \frac{\partial^2 u}{\partial y^2} + \frac{1}{3}\left(\frac{\partial^2 u}{\partial x^2} + \frac{\partial^2 v}{\partial x \partial y}\right)\right) = 0 \tag{2}$$

Conservation of y- momentum:

$$\frac{\partial \rho v}{\partial t} + u\frac{\partial \rho v}{\partial x} + v\frac{\partial \rho v}{\partial y} + \frac{\partial P}{\partial y} - \mu\left(\frac{\partial^2 v}{\partial x^2} + \frac{\partial^2 v}{\partial y^2} + \frac{1}{3}\left(\frac{\partial^2 v}{\partial y^2} + \frac{\partial^2 u}{\partial x \partial y}\right)\right) = 0 \tag{3}$$

Conservation of energy:

$$\begin{aligned} &\rho Cp \frac{DT}{Dt} - \frac{DP}{Dt} - \frac{\partial}{\partial x}\left(k\frac{\partial T}{\partial x}\right) - \frac{\partial}{\partial y}\left(k\frac{\partial T}{\partial y}\right) \\ &\quad -\mu\left(2\left(\frac{\partial u}{\partial x}\right)^2 + 2\left(\frac{\partial v}{\partial y}\right)^2 + \left(\frac{\partial v}{\partial x} + \frac{\partial u}{\partial y}\right)^2 - \frac{2}{3}\left(\frac{\partial u}{\partial x} + \frac{\partial v}{\partial y}\right)^2\right) = 0 \end{aligned} \tag{4}$$

The pressure is defined using the perfect gas law,

$$P = \rho RT \tag{5}$$

The "no-slip" wall condition is defined as having all components of the velocity vanish at the solid wall. However, as the Knudsen number increases, this description becomes vague and the walls start to "move". At this stage, streaming velocity at the wall comprises the streaming velocity of incident particles and that of the scattered particles. The slip relations of Maxwell[19] for dilute, monoatomic gases has been implemented in the momentum equation as,

$$u_g - u_w = \frac{2-\sigma_V}{\sigma_V}\lambda\left(\frac{\partial u}{\partial y}\right)_w + \frac{3}{4}\frac{\mu}{\rho T_g}\left(\frac{\partial T}{\partial x}\right)_w \tag{6a}$$

Eqn. (6a) can be modified to the following form based on the definition of Kn,

$$-\mu\left(\frac{\partial u}{\partial y}\right)_w = \frac{5\rho\sigma_V\sqrt{2\pi RT}}{16(2-\sigma_V)}\left(u_w - u_g + \frac{3}{4}\frac{\mu}{\rho T_g}\left(\frac{\partial T}{\partial x}\right)_w\right) \tag{6b}$$

Corresponding temperature-jump relation for the energy equation was derived by von Smoluchowski[20] as

$$T_g - T_w = \frac{2-\sigma_T}{\sigma_T}\left[\frac{2\gamma}{\gamma+1}\right]\frac{\lambda}{\Pr}\left(\frac{\partial T}{\partial y}\right)_w \tag{7a}$$

Eqn. (7a) can also be modified as,

$$-k\left(\frac{\partial T}{\partial y}\right)_w = \frac{\sigma_T\sqrt{2\pi RT}}{2-\sigma_T}\left[\frac{\gamma+1}{2\gamma}\right]\frac{5\rho C_p}{16}\left(T_w - T_g\right) \tag{7b}$$

In Eqns. (6)-(7), u_g and T_g are the velocity and temperature of the gas adjacent to the wall, while u_w and T_w are the velocity and temperature at the wall. The tangential-momentum accommodation coefficient, σ_V and the thermal accommodation coefficient, σ_T at the walls indicate the molecular fraction reflected diffusively from the walls. The second term in the eqn. (6a) is known as thermal creep, which generates slip velocity in the direction opposite to the increasing temperature.

Traditionally, the first order equations (6-7) are applied as long as Kn < 0.1. Karniadakis & Beskok[2] has presented a higher order slip boundary condition, which is second order accurate, for predicting flow accurately for higher Knudsen number in the transition regime. It has been suggested that Maxwell's first order boundary condition breaks down near Kn = 0.15 (Sreekanth[25], Piekos & Breuer[26]). However, Roy *et al*.[21] have successfully utilized the first-order boundary condition for higher Knudsen number of up to 7.36 and it has also been suggested that the higher order slip boundary conditions may actually deviate from the actual solution more than the first order Maxwell's wall-slip conditions[19]. Due to these reasons, we would restrict slip to first order conditions (6-7).

FINITE ELEMENT FORMULATION

The system of eqns. (1-5) can be represented in more concise form as

$$L(\boldsymbol{q}) = \frac{\partial \boldsymbol{q}}{\partial t} + \frac{\partial\left(\boldsymbol{f}_j - \boldsymbol{f}_j^v\right)}{\partial x_j} - s = 0 \ \ , 1 \le j \le 2 \qquad (8a)$$

$$\boldsymbol{q} = \begin{pmatrix} \rho \\ \rho u_i \\ \rho C_p T + P \\ 0 \end{pmatrix}, \boldsymbol{f}_j = \begin{pmatrix} \rho u_j \\ u_j \rho u_i + P\delta_{ij} \\ u_j(\rho C_p T + P) \\ 0 \end{pmatrix},$$

$$\boldsymbol{f}_j^v = \begin{pmatrix} 0 \\ \tau'_{ij} \\ k\dfrac{\partial T}{\partial x_j} + \tau'_{ij} u_i \\ 0 \end{pmatrix}, s = \begin{pmatrix} 0 \\ 0 \\ 0 \\ P - \rho R T \end{pmatrix}, \quad 1 \le i \le 2 \qquad (8b)$$

where $\boldsymbol{q}$ is the state variable, $\boldsymbol{f}$ is the kinetic flux vector, $\boldsymbol{f}^v$ the dissipative flux vector and s is the source term; and $\tau'_{ij} = \mu\left(\frac{\partial u_i}{\partial x_j} + \frac{\partial u_j}{\partial x_i}\right) + \delta_{ij}\lambda\frac{\partial u_k}{\partial x_k}, \ \ 1 \le i,j,k \le 2\cdot$

The difficulty involved in achieving a steady state solution for eqns. (8a-b) directly is due to the selection of initial conditions. The conventional method of achieving a steady state solution is to use the time term as a relaxation parameter in the equation system and run the problem till the transient features die down. Here we utilize an artificial diffusion term as an initial condition generator to obtain a final steady state solution.

Eqn. (8) can be modified in the following steady state form,

$$L(\boldsymbol{q}) = \frac{\partial\left(\boldsymbol{f}_j - \boldsymbol{f}_j^v\right)}{\partial x_j} - \beta\frac{\partial^2 \tilde{\boldsymbol{q}}}{\partial x_j^2} - s = 0 \ \ , 1 \le i, j \le 2 \qquad (9)$$

where, $\tilde{\boldsymbol{q}}^T = \left(0, u_i, T, 0\right)$ and β is a diffusion perturbation parameter that can be varied separately for each state variable. As $\beta \to 0$, eqn. (9) reverts back to steady state form of equation (8). Initially β is set to a sufficiently high value so as to generate a diffused but stable convergence to steady state solution. Progressive reduction of β is carried out till the final steady state solution with $\beta \to 0$ is achieved. This procedure is analogous to using the transient relaxation.

Using any admissible test function w, the variational integral yields the *weak statement (WS)* for equation (9). Thereafter, the domain Ω and integrated variables $\boldsymbol{q}$ are spatially discretised (Ω_e and $\mathbf{Q}$) using Lagrange basis functions N_k complete to the degree k.

$$WS = \int_\Omega wL(\boldsymbol{q})\, d\Omega = 0, \ \Rightarrow WS^h = S_e\left(\int_{\Omega_e} N_k L_e(\mathbf{Q})\, d\tau\right) \equiv 0 \qquad (10a)$$

$$WS^h = S_e\left(\begin{array}{c} \displaystyle\int_{\Omega_e} N_k(-s)\, d\tau - \int_{\Omega_e} \frac{\partial N_k}{\partial x_j}\left(\boldsymbol{f}_j - \boldsymbol{f}_j^v\right)_e d\tau + \\ \displaystyle\oint_{\partial\Omega_e \cap \partial\Omega^h} N_k\left(\boldsymbol{f}_j - \boldsymbol{f}_j^v\right)_e \hat{n}_j d\sigma \end{array}\right) \qquad (10b)$$

In (10), the superscript h denotes discretization and S_e symbolizes the "assembly operator" carrying local (element e) matrix coefficients into the global arrays. The weak statement naturally yields the surface integrals via application of Green-Gauss theorem in equation (10), which contains the unknown boundary fluxes wherever Dirichlet (fixed) boundary conditions are enforced. The zero gradient boundary conditions are automatically enforced via removal of the surface integral. For the slip flow boundary, appropriate surface integrals are replaced by incorporating the eqns. (6b) and (7b) into the momentum and energy equations. Independent of the physical dimension of Ω, and for general forms of the flux vectors, the semi-discretized weak statement of equation (10) always yields an ordinary differential equation (ODE) system. The terminal ODE is usually solved using a Newton-Raphson scheme.

The computational channel geometry is discretized using two-dimensional non-overlapping 9-noded biquadratic finite elements. The continuity and equation of state are solved for density and pressure respectively using the four corner nodes of the element. For velocity and temperature calculations, all nine nodes of the biquadratic element are used.

Boundary Conditions

For Case 1 the gas temperature T_0 at the inlet, and an isothermal wall temperature T_w are specified. At the inlet the velocity flux is $\partial u/\partial x=0$ and the y-component of the velocity is $v = 0$. The pressure at the outlet, P_0 is 101 kPa and the inlet pressure, P_i is specified based on the corresponding pressure ratio. The microchannel is benchmarked using both no-slip and first order slip conditions.

For high speed flows (Case 2 and 3) the inlet boundary is fixed for velocity u_0 (based on Mach number, Ma_0), temperature T_0 and the density ρ_0 (based on inlet pressure, P_0) as listed in Table 1. The wall temperature for the top and the bottom surface is set to be T_w. The velocity flux is $\partial u/\partial x=0$ at the outlet and the *y*-component of the velocity *v* vanishes at the inlet. A backpressure equal to the inlet boundary pressure is specified at the outlet. The drawback faced for modeling this problem is that outflow boundary conditions could not be replicated since the exact location of the outlet pressure is not clear in any of the references.[13,14] We specify a backpressure $P_0 = 1.01 \times 10^5$ Pa, 0.2 μm downstream from the exit.

Near the entrance, the wall boundary for the length ***B*** ("lighter wall") is defined by the accommodation coefficients of $\sigma_V = \sigma_T = 0.0$, implying a specular reflection where only the tangential component of velocity of the impinging molecules is conserved making it a freestream region. In the rest of the domain ("darkened walls"), the gas to wall interaction is set with $\sigma_V = \sigma_T = 1.0$ implying the gas molecules undergo a complete change in momentum after collision.

RESULTS AND DISCUSSION

Case 1 is based on experimental measurement of mass flow rates for Helium gas (Arkilic *et al.*[9]). The microchannel has an aspect ratio of 5639 having a length of 7500 μm and 1.33 μm height. It was manufactured using a two-wafer manufacturing process by etching an oxide grown on silicon. The outlet condition is atmospheric. Five different pressure ratios are used between 1.340 and 2.701 with a maximum Knudsen number of 0.155 (transition regime) at the outlet. The computational geometry is discretized using 560 two-dimensional bi-quadratic elements consisting of 2337 nodes.

For five different pressure ratios, the pressure distribution shows a non-linear trend. The pressure drops in order to overcome the shear stresses within the channel. The numerical slip and no-slip pressure trends show a maximum difference of 4%. With a slip boundary the flow encounters lesser frictional forces on the wall than no-slip boundary, which tends to make the slip flow more linear as compared to the no-slip flow.

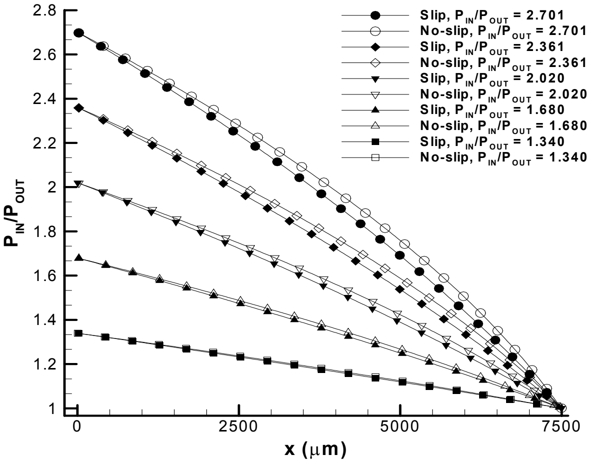

Figure 2. *Comparison of the centerline pressure distribution for slip and no-slip results.*

The temperature variation in the channel is found to be negligible indicating that the density variation is proportional to the pressure change. Due to mass flux conservation, velocity increases as the density and pressure drop; however the values remain considerably low indicating a sub-sonic flow, Figure 3. The small knee noticeable near the outlet for streamwise velocity solution is due to the imposed vanishing gradient boundary condition. The crosswise direction cuts taken at three points for P_{in}/P_{out} = 2.701 along the channel, plotted in Figure 4, show the difference in the wall velocities. The wall velocity at x = 5625 μm is approximately 50% more than that at x= 1875 μm. As Kn increases due to lower density downstream, the slip effect increases.

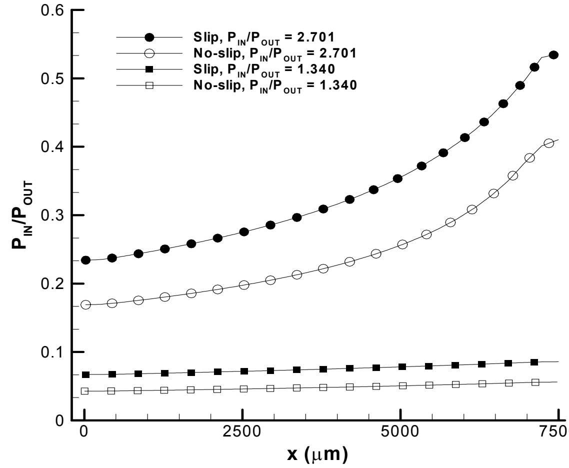

Figure 3. *Comparison of the centerline slip and no-slip velocity solutions for* P_{in}/P_{out}*=1.340 & 2.701.*

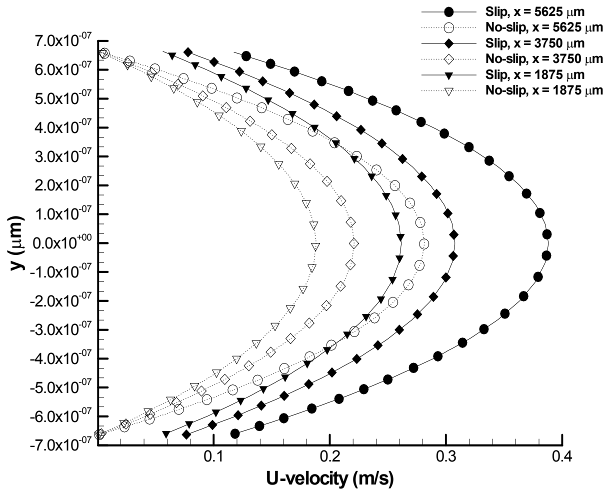

Figure 4. *Comparison U-velocity for slip and no-slip condition in the y-direction at three different sections along the length of the microchannel for* P_{in}/P_{out}*=2.701.*

The only experimental data available for this case is the mass flow rate, which has been compared with the slip and no-slip solutions. Figure 5 compares mass flow rates for different pressure ratios with both experimental data[9] and numerical solution.[24] The computed mass flow rate for the slip condition is ~35% higher than no-slip boundary. The predicted slip flow results differ by only ~+2.5% with numerical slip-solution and a maximum of +7% from the experimental data.

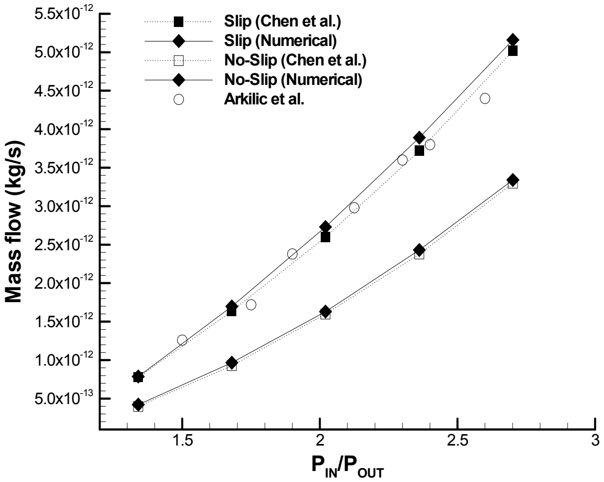

Figure 5. *Computed mass flow rate (kg/s) compared with the experimental data of Arkilic et al.*[9] *and the numerical slip and no-slip mass flow rates from Chen et al*[24]*.*

For Cases 2 and 3, a single computational grid consisting of 560 finite elements and 3485 nodes is used for simulating the high-speed gas flow. The length scale is normalized based on the height of the channel. The extra length of 0.2 μm is ignored downstream for both cases while presenting the results. The Knudsen number for Case 2 is 0.14 and for Case 3 it is 0.062.

The streaming velocity contours for Case 2 (helium) and Case 3 (nitrogen) are shown in Figure 6. The U-velocity for Case 2 remains constant in the "lighter" region and drops down further downstream, figure 6(a), creating bow shock structure around x/H = 3.0. Contrarily, for Case 3 the U-velocity contours extend downstream with no presence of any shock as plotted in figure 6(b). Figure 7 plots the pressure contours for Cases 2 and 3. The pressure contours for Kn = 0.14 show the dominance of the backpressure near the exit. The shock waves stemming from the leading edges and the exit meet at x/H = 3.2, Figure 7(a). The effect of backpressure is minimal for Kn = 0.062 shown in figures 6(b), 7(b), 8(b), where nitrogen is used as working fluid. The density contours shown in

Figure 8 have similar profile as that of the pressure for both cases. Clearly, the fluidity of helium makes it more interesting with shock-wall layer interactions. A sharp density rise follows the pressure rise.

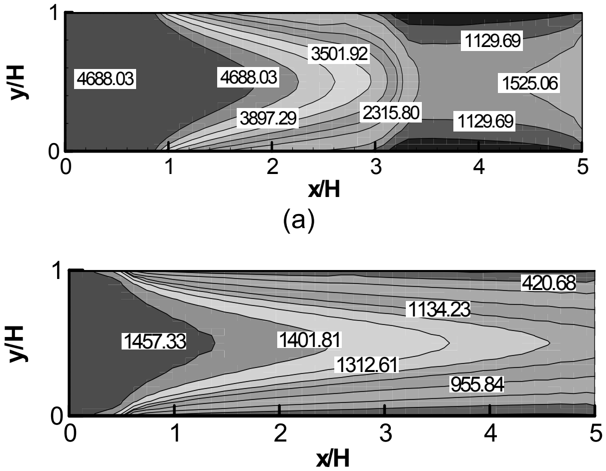

(a)

(b)

Figure 6. *U velocity contours for (a) Kn = 0.14 and (b) Kn = 0.062*

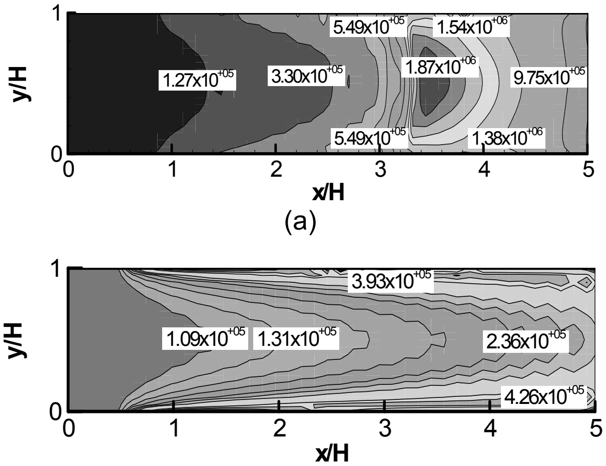

(a)

(b)

Figure 7. *Pressure contours for (a) Kn = 0.14 and (b) Kn = 0.062.*

Since no experimental data is available for these cases, the first order Navier-Stokes solution is compared with reported DSMC results[13] for Kn = 0.14. However, the centerline profiles are not available for comparison for Kn = 0.062. Figure 9 compares the hydrodynamic solution of U-velocity, pressure and density distribution at the channel centerline with the DSMC results.[13] The presence of back pressure plays a dominant role in determining the solution characteristic. Comparison in figure 9(a) shows steady drop in downstream U-velocity for DSMC indicating a more diffused solution. Similar trend is seen for pressure and density, Figures 9(b)-(c), reflecting a steady rise. Contrarily, the hydrodynamic solutions captures a sharp shock around x/H = 3.2. Note that the inlet Mach number for Case 2 is 5.0.

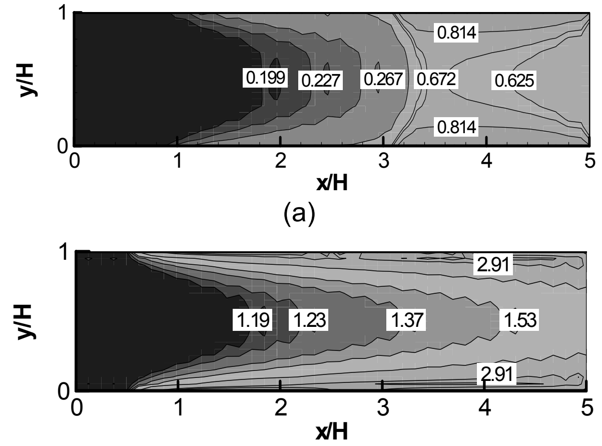

(a)

(b)

Figure 8. *Density contours for (a) Kn = 0.14 and (b) Kn = 0.062.*

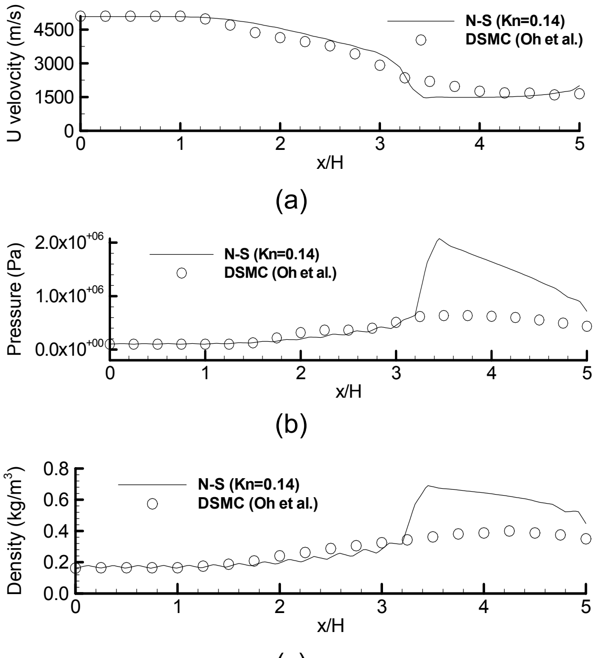

(a)

(b)

(c)

Figure 9. *Comparison of centerline distribution of N-S solutions for Kn = 0.14 with available DSMC results[13] for, (a) U-velocity, (b) pressure and (c) density.*

Figure 10 plots the solution prediction near the wall along the streamwise direction to indicate the slip effects for Case 2 with Kn = 0.14. The U-velocity near the wall varies between 5000 m/s to 1000 m/s with Mach number ranging from 5.0 to nearly 1.0 due to presence of velocity slip and temperature jump. The dominance the shock due to the backpressure is visible both in the case of pressure and density, Figures 10(b)-(c). The shock emanating from the walls is the highest near x/H=3.2. Specifically for pressure and density the values beyond the shock are much higher as compared to DSMC predictions.

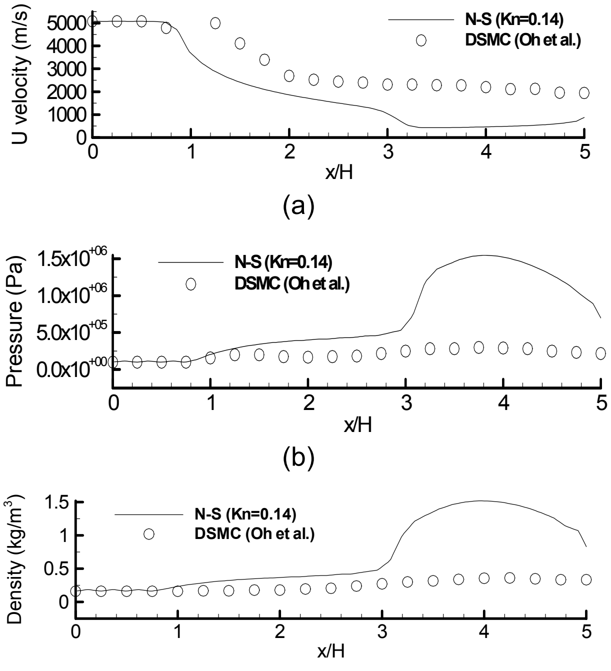

(a)

(b)

(c)

Figure 10. *Comparison of near wall distribution of N-S solutions for Kn = 0.14 with available DSMC results*[13] *for; (a) U-velocity, (b) pressure and (c) density.*

The centerline distributions for Case 3 with Kn = 0.062 is presented in Figure 11. Due to the lack of available data in the literature, they are not compared with any published reports. The inlet Mach number for this case is 4.15, which steadily decreases to 2.5 at the outlet. Corresponding U velocity, pressure and density distributions are predicted in Figures 11 (a)-(c), respectively. The results show less presence of shock-like features for Nitrogen with lower Knudsen number flow. Near the wall, however, steeper features are documented as shown in Figure 12 (a)-(c). The U-velocity drops steeply after the freestream region to a relatively steady value. On the other hand the pressure and density reflect the presence of shock structures near the leading edges of the channel, as shown in figure 12(b)-(c).

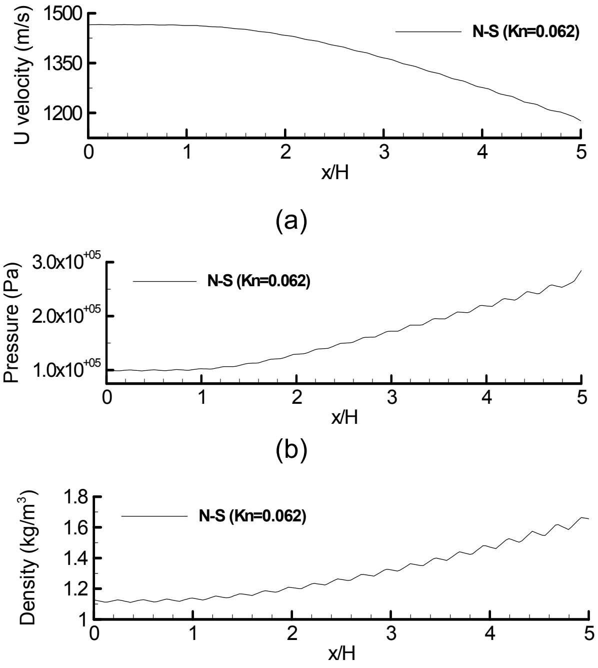

(a)

(b)

(c)

Figure 11. *Comparison of centerline distribution of N-S solutions for Kn = 0.062 of, (a) U-velocity, (b) pressure and (c) density.*

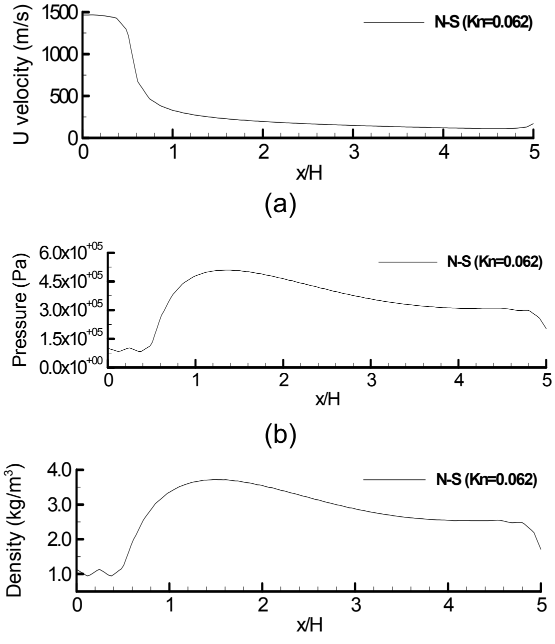

(a)

(b)

(c)

Figure 12. *Comparison of near wall distribution of N-S solutions for Kn = 0.062; (a) u velocity, (b) pressure and (c) density.*

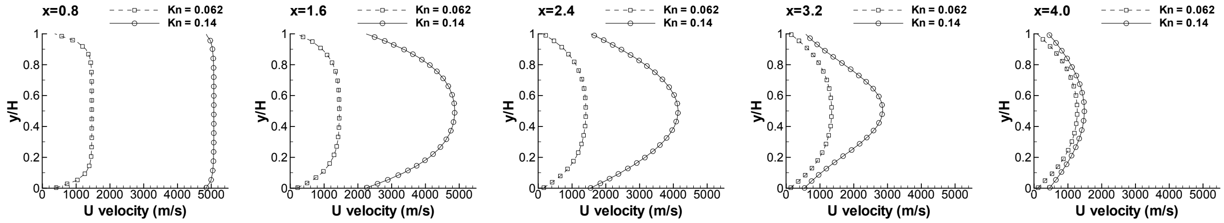

Figure 13. *U-velocity distribution along the y-direction for different cross-sections along the channel for Kn = 0.14 and Kn = 0.062.*

Figure 13 shows comparison of the velocities on five planes in the crosswise direction for Kn = 0.14 and 0.062. Sections have been taken at x/H =0.8, 1.6, 2.4, 3.2, 4.0 locations. For Kn = 0.14 at x/H = 0.8, the U-velocity near the center remains nearly the inlet value. Similar trend is shown for Kn = 0.062. However, the profiles differ due to different lengths for ***B***. For Kn = 0.14, sharper drop in velocity takes place and the profile tends to become less parabolic near the exit region. However, for Kn = 0.062 the drop is relatively flatter without much change in the parabolic profile. For both the cases higher velocity reflects more slip on the walls.

CONCLUSIONS

The finite element based hydrodynamic model yields reasonably accurate solution for flows within transition regime. The mass fluxes for low speed flows compare within +2.5% with reported numerical results and show a maximum difference of +7% with the experimental data. On the other hand, although hydrodynamic solutions for high speed flows differ slightly in values the profiles obtained are similar to that of the reported DSMC results. Specifically, the hydrodynamic model with first order slip boundary conditions was able to capture sharp shock and wall interaction features for the supersonic flows through the microchannel.

REFERENCES

[1]Ho, C.M. and Tai, Y.C., 1998, “Micorelectromechanics systmes(MEMS) and fluid flows,” *Annu. Rev. Fluid Mech,* vol. 30, pp. 579-612.

[2]Karniadakis, G. and Beskok, A., 2002, “Micro Flows-Fundamentals and Simulation”, *Springer-Verlag New York, Inc.*

[3]Schaaf, S.A. and Chambre, P.L., 1961, “Flow of rarefied gases,” *Princeton University Press, Princeton, New Jersey.*

[4]Pfahler, J., Harley, J., & Bau, H., 1990, “Liquid Transport in Micron and Submicron Channels,” *Sensors and Actuators,* A21-A23, pp. 431-434.

[5]Harley, J.C., Huang, Y. and Bau, H., 1995, “Gas flow in microchannels.” *Journal of Fluid Mechanics,* vol. 284, pp. 257-274.

[6]Liu, J., Tai, Y. C., Pong, K. and Ho, C. M., 1993, “Micromachined channel/pressure sensor systems for micro flow studies”, *The 7th International Conference on Solid-state Sensors and Actuators*, *Transducers’93,* pp.995-998.

[7]Pong, K.C., Ho, C., Liu, J. and Tai, Y.C., 1994, “Non-linear pressure distribution in uniform microchannels.” *Application of Microfabrication to Fluid Mechanics,* FED – 197, pp.51-56.

[8]Shih, J.C., Ho, C.M., Liu, J. & Tai, Y.C., 1996, “Monatomic and polyatomic gas flow through uniform microchannels,” *ASME* DSC 59,pp.197-203.

[9] Arkilic, E.B., Breuer, K.B. & Schimidt, M.A, 1994, “Gaseous Flow in Microchannel,” *Application of Microfabrication to Fluid Mechanics, ASME,* FED-197, pp. 57-66.

[10]Arkilic, E.B., Schimidt, M.A. and Breuer, K.B., 1997, “Gaseous slip flow in long microchannels”, *Journal of Microelectromechanical systems,*vol. 6, no. 2, pp. 167-178.

[11]G. A. Bird, 1994, “Molecular Gas Dynamics and the Direct Simulation of Gas Flows,” *Clarendon Press, Oxford, United Kingdom*.

[12]D. Burnett, 1935, “ The distribution of molecular velocities and mean motion in a nonuniform gas,” *Proc. London Math. Soc.*, vol.40, pp. 382-435.

[13]Oh C.K., Oran E.S. and Sinkovits R.S., 1997, “Computations of High speed, High Knudsen number Microchannel flows”*, Journal of Thermophysics and Heat Transfer,* vol. 11, pp. 497-505.

[14]Liou, W.W and Fang, Y., 2001, “Heat Transfer in Microchannel devices using DSMC”, *Journal of Microelectromechanical Systems*, vol.10, no.2, pp.274-279.

[15]Mavriplis, C., Ahn, J.C. and Goulard, R., 1997, “Heat Transfer and flowfeilds in Short Microchannels using Direct Simulation Monte Carlo,” *Journal of Thermophysics and Heat Transfer,* vol. 11, no. 4, pp. 489-496.

[16]Agarwal, R.K., Yun, K. and Balakrishnan, R., 2001, “Beyond Navier-Stokes: Burnett equations for flows in the continuum-transition regime”*, Physics of Fluids,* vol. 13, no. 10, pp. 3061-3085.

[17]Gad-ek-hak, M., 1999, “The Fluid Mechanics of Microdevices- The Freeman Scholar Lecture”, *Journal of Fluids Engineering,* vol.121, pp. 5-33.

[18]Oran, E.S., Oh, C.K. and Cybyk, B.Z., 1998, ”Direct simulation Monte Carlo: Recent advances and applications,” *Annu. Rev. Fluid Mechanics,* vol. 30, pp. 403-441.

[19]Maxwell, J.C.,1879, “On stresses in rarefied gases arising from inequalities of temperature”, *Philosophical Transactions of the Royal Society Part 1,* vol.170, pp.231-256.

[20]Smoluchowski, von M., 1898, “Ueber wärmeleitung in verdünnten gasen”, *Annalen der Physik und Chemi,* vol. 64, pp. 101-30.

[21] Roy, S., Raju, R., Chuang, H., Cruden, B. and Meyyappan, M., 2003, “Modeling gas flow through microchannels and nanopores,” Journal of Applied Physics, vol.93, no. 8, pp. 4870-79.

[22]Lockerby,D.A. and Reese, J.M., 2003, “High resolution Burnett simulations of micro Couette flow and Heat Transfer,” *Journal of Computational Physics*, (article in press).

[23]Raju ,R., Pandey, B.P. and Roy S., 2002, “Finite Element Model of Fluid Flow inside a Micro-Thruster”, *Nanotech 2002 - "At the Edge of Revolution", Houston, Texas* ,AIAA-2002-5733.

[24]Chen, C.S., Lee, S.M. and Sheu J.D., 1998, “Numerical Analysis of Gas flow in Microchannels”, *Numerical Heat Transfer, Part A,* vol. 33,pp.749-762.

[25]Sreekanth, A.K., 1969, “Slip Flow through Long Circular Tubes”, *Rarefied Gas Dynamics, eds. Trilling, L. and Wachman, H. Y., Academic Press, New York* **,**vol. 1, pp. 667-680,

[26]Piekos, E. & Breuer, K., 1995, “DSMC modeling of microchannel devices,” *AIAA Thermophysics Conference, San Diego, CA,* AIAA 95-2089.